Hindawi
Adsorption Science & Technology
Volume 2022, Article ID 7423102, 14 pages
https://doi.org/10.1155/2022/7423102

Research Article

Synthesis and Adsorbent Performance of Modified Biochar with Ag/MgO Nanocomposites for Heat Storage Application

R. Venkatesh,[1] **N. Karthi**,[2] **N. Kawin**,[3] **T. Prakash**,[4] **C. Ramesh Kannan**,[5] **M. Karthigairajan**,[6] **and Ketema Bobe**[7]

[1]*Department of Mechanical Engineering, Saveetha School of Engineering, SIMATS, Chennai, 602105 Tamil Nadu, India*
[2]*Department of Mechatronics Engineering, SNS College of Technology, Coimbatore, 641035 Tamil Nadu, India*
[3]*Department of Mechanical Engineering, Kongunadu College of Engineering and Technology, Trichy, 621215 Tamil Nadu, India*
[4]*Department of Mechanical Engineering, SNS College of Technology, Coimbatore, 641035 Tamil Nadu, India*
[5]*Department of Mechanical Engineering, Dr. Navalar Nedunchezhiyan College of Engineering, Tholudur, 606303, Tamil Nadu, India*
[6]*Department of Mechanical Engineering, Gojan School of Business and Technology, Chennai, 600052 Tamil Nadu, India*
[7]*Department of Mechanical Engineering, Ambo University, Ambo, Ethiopia*

Correspondence should be addressed to Ketema Bobe; ketema.bobe@ambou.edu.et

Received 26 July 2022; Revised 4 September 2022; Accepted 10 September 2022; Published 29 September 2022

Academic Editor: Debabrata Barik

Heat storage is a major problem in the world. Many research is going on the heat storage application. This research investigates the novel Ag/MgO/biochar nanocomposites for heat storage. Ag/MgO/biochar nanocomposites were fabricated using solvent-free ball milling techniques. According to several analytical measurements, the Ag/MgO nanoparticles in biochar are uniformly dispersed across the carbon interface. This type of adsorbent material has been characterized by different techniques such as X-ray diffraction pattern analysis (XRD), FTIR analysis, scanning electron microscope (SEM), and transmission electron microscope (TEM) as all indicate the surface morphology and successful ball milling synthesis of Ag/MgO nanocomposites. The UV visible spectroscopy wavelength range of AgNPs and MgONPs is 330 nm and 470 nm, respectively. FTIR analysis revealed that different functional groups of modified biochar nanocomposites such as O-H group are 3728 cm^{-1} and for C-H bond is 932 cm^{-1}, C-O group is 1420 cm^{-1}, and C=O is 1785 cm^{-1}, respectively. Adsorption tests showed that 1.0 gL^{-1} dosage with 60% phosphate removal, an ion, and 0.2 gL^{-1} of dosages that had 85% methylene blue decomposition, a charged synthetic dye, were the lowest absorption levels. This research suggests that ball milling offers the advantages of stabilization and chemical adaptability for customized remediation of different atmospheric contaminants. Ball milling is a facile and feasible process to fabricate carbon-metal-oxide nanomaterials.

1. Introduction

Due to its low cost, high efficiency, and ease of implementation, the adsorption technique is one of the most effective techniques for removing organic dyes from water [1]. Recent research has extensively investigated the effects of adsorption and photocatalytic techniques on metal oxide/biochar nanocomposites [2]. Water pollution is one of the main causes of eutrophication, environmental threats, human welfare, and animal planet. Wastewater reclamation is required for various applications as a financially sustainable and effective technologies for removing unwanted contaminants. In terms of wastewater generation, this strategy is a better option in light of the emergence of renewable techniques [3, 4]. This approach has gained importance among most of the country's population due to the groundwater issues crisis due to fluctuating precipitation and uneven access to many freshwater resources, particularly for farming. Adsorption process, catalysis, improved oxidative degradation, electrochemical analysis, and microbial degradation are among a few of the remediation techniques invented to reduce the hazards brought on by natural dyes.

Depending on the pH value, phosphorus in different forms of the critical nutrients PO43-, H2PO4-, and HPO42 enhances aquatic plants growth [5–7]. In general, biochar (BC) has low adsorption capacity due to restricted adsorption location, low area of surface impact, and negatively discharged surface on phosphorus [8, 9]. Solid BC is produced by biomass using the pyrolysis method under low oxygen (no oxygen) environmental conditions at high temperatures. To develop the adsorption, modification of BC with various MO, such as La2O3, CaO, and MgO, is of great importance. Biochar surface modification is performed by impregnation fabrication techniques, which have high adsorption capacity and high phosphorus removal from various water resources. For biomedical applications, excellent features such as ease of fabrication, recyclability, and surface functionalization have allowed biochar to be used in various industries. Several studies have revealed that MgO exhibits effective adsorption measurements for decreasing PO_4^{3-} from water. The maximum absorption coefficient was obtained at 121.25 mgg^{-1} for MgO modified biochar using the impregnation technique investigated by Li et al. [7, 8]. Rather than standard impregnation, the emerging ball milling approach is a solvent-free modification technique that requires adding oxides to the modified biochar surface [10, 11].

The synthesis of nanocomposites through ball milling approaches is the most widely recognized technique that improves the physical and chemical properties of metal oxide with biochar nanocomposites [12, 13]. The physical properties of the nanomaterials can be enhanced by ball milling the composites into nanoparticles, which will improve the overall ability to adsorption capability [13, 14]. The modified biochar composites (CuO, MgO, and Fe_3O_4) with different metal oxides were fabricated through ball milling for disposal of methylene blue from the water content [15]. According to the observations of those investigations, ball milling provides a large surface area and chemical bonding of the biochar [16, 17], which allows the nanocomposite produced from biochar-containing metal oxides to have better removal efficiency than pure biochar.

For the first time, Persicaria salicifolia biomass was investigated to support less harmful chemical compounds as natural and eco-friendly chemicals for phytofabrication of zinc oxide-silver sponsored activated carbon nanocomposite (Ag/ZnO@BC). About 20 nm in diameter and spread evenly on the surface of the biochar substrate, MgO nanoparticles were used in the nanocomposite to create nanoscaled geometries and microporous structures, according to the physicochemical parameters of the prepared nanostructured materials. MgO/biochar nanomaterials were prepared using a simple ball milling technique to provide dual adsorption. At moderate adsorbent concentrations of 1.0 g L-1 and 0.2 g L-1, adsorption tests showed 62.9% removal of phosphorus, 87.5% removal of methylene blue, and charged molecular dye. Desorption capacity of this novel nanocomposite as photocatalysts in various systems revealed its strong photodegradation efficiency, which reached 70.3% under optimal process parameters: 50 ppm of TC, pH 6, 0.01 g of Ag/ZnO@BC, 25°C temperature, and 100 mM H_2O_2 relative to parameters.

The synthesis of MgO nanoparticles with Ag is the preparation of modified biochar materials through solvent-free ball milling techniques, which is the main innovation of this investigation. In this study, inspired by the research above, modified Ag/MgO/biochar nanocomposites were fabricated by ball milling process followed by ball milling techniques and phosphorus elimination from pollutant water. Subsequently, the experimental study aimed to investigate (i) the properties of modified Ag/MgO/biochar nanocomposites, (ii) effect of AgNPs and MgONPs on Escherichia coli pneumonia, including S. aureus and E. coli species of antibacterial activity, (iii) scanning electron microscope (SEM) and transmission electron microscope (TEM) studies reveal the surface morphological changes on biochar nanocomposites, and (iv) adsorption performance of removal of methylene blue (MB) and phosphates by using Ag/MgO/biochar nanocomposites.

2. Materials and Methods

2.1. Materials. Silver nitrate ($AgNO_3$) -99.9% and magnesium chloride hexahydrate ($MgCl_2.6H_2O$) synthesized the Ag/MgO biochar nanocomposites.

2.2. Synthesis of Biochar Ag/MgO Biochar. 5 g of rice straw powder was mixed with 0.175 g of magnesium chloride hexahydrate ($MgCl_2.6H_2O$) and 0.08 g of $Ag.NO_3$ for Mg : Ag weight ratio is 1 : 1 and 3 : 1 wt% ratio for Ag : BC and Mg : BC, respectively. This solution was then mixed with 100 mL of deionized water, and the samples were diluted for approximately 30 minutes, stirred for an additional 30 minutes, and heated to 70°C. The mixture was further dried completely at 60°C. Dry rice straw powder was oxidized in an electric furnace at 600°C for three hours to convert MgO and Ag ions into MgONPs and AgNPs. This produced the biochar element, which was used to create unique biocomposites (Ag/MgO@BC), which were finally obtained. Figure 1 shows the detailed flow chart for synthesising modified biochar nanocomposites.

2.3. Characterization of Modified Ag/MgO Biochar. The photosynthesis of Ag/MgO with biochar absorption quantitative measurement was confirmed by UV-visible spectroscopy (IG-28 ms). The wavelength range for UV analysis is 665 nm was followed. Furthermore, the elemental compositions of modified biochar surfaces were analyzed by energy-dispersive spectroscopy (EDS). These XRD patterns reveal the crystalline structure of nanocomposites under Cu kα radiation ($\lambda = 0.154$ nm), which functioned at 40 kV to 40 mA. SEM and TEM performed at 5.0 kV and 80 kV were used to study the surface morphology, chemical compositions, and elemental analysis of the proposed biochar samples. FT-IR measurements were obtained using TENSOR-5, Bruker FTIR spectroscopy in the spectrum range of 4000-400 cm^{-1}. TGA experiment was completed with the help of Pyris-1, Diamond TG/DTA PerkinElmer analyzer. Zeta PALS, Brookhaven, was used to measure the zeta potentials of the prepared materials to evaluate their surface properties and sustainability.

Figure 1: Fabrication of Ag/MgO/biochar nanocomposites.

2.4. Heat Storage Adsorption Mechanism. Dissolving K_2HPO_4 (potassium phosphate) and $NaNo_3$ (sodium nitrate) in 100 ml distilled water to prepare the nitrate and phosphate solutions, respectively. Also, the adsorption of phosphate to nanomaterials was evaluated by measuring the phosphorus concentration of 50 mg of each sample in 20 mg L-1 solution (B). The feedstock 1800 ml/L P and 40 mg/LN was prepared for the adsorption experiment and carried out at room temperature (220 C) using 65 mL digestion vessels. During the filtration process, excitation-correlated ionized atomic emission spectroscopy was used to determine P levels. The solutions were finally passed through 0.25 μm nylon membrane, and the MB dosage of the filtrates was determined using UV–visible spectroscopy with a frequency range of 700 nm. Also, MB and P were used as treatments for adsorption experiments, which were carried out in similar conditions. Summary statistics from each experiment were presented after repeated runs. New tests were performed each time there was a measurement variation of 5%.

3. Results and Discussion

3.1. UV Visible Spectroscopy. The surface plasmonic resonance (SPR) of Ag/MgO/biochar excited by a light source at specific wavelengths was recorded using wavelength-distinct UV-visible spectroscopy as shown in Figures 2(a) and 2(b). SPR peak intensities determine morphological changes through the shape and size of nanoparticles. The SPR spectra reveal that no band is identified in the modified biochar. The UV visible range of AgNPs and MgONPs is 330 nm and 470 nm, respectively, representing the surface decrease of silver ions and magnesium oxide in BC and the formation of biochar nanocomposites. The measured AgNPs SPR band was consistent with a previous study aimed at developing silver nanoparticle-based nanocomposites [18]. In addition, as can be seen in Figure 2(c), the energy band gap energy (Eg) of Ag/MgO with BC was determined using the Tauc plot and 3.4 eV-3.12 eV. According to Saedi et al., the energy band gap became very narrow due to the addition of MgO and Ag nanoparticles in the nanostructure [19]. Due to the synthesis of Ag-C compounds, the precipitation of MgONPs and AgNPs on the biochar surface narrows the frequency wavelength energy band gap of specific BC. It accelerates the development of stable energy levels in Ag/MgO/BC, as a result of the interface of AgNPs through the carbon in the biochar [20].

3.2. FT-IR Analysis. The functional group found by the oxidation and normalisation of photocatalyzed nanoparticles is revealed by FTIR analysis. From the analysis, three kinds of functional group were observed in modified biochar such as O-H group is 3728 cm-1, the C-O bond is 932 cm-1, the C-O group is 1420 cm^{-1}, and C=O is 1785 cm^{-1}, respectively. Zheng et al. [21] have achieved that the biochar produced spectra comparable to Ag/MgO biochar and demonstrated that adding MgO nanoparticles to the composites did not affect the functional groups of the biochar. These patterns, which also appeared in the Ag/biochar and MgO/biochar spectra with various strengths, decreased both AgNPs and MgONPs on the biochar surface. Additionally, a novel MgO maximum intensity was detected in the MgO/biochar composite at 632 cm^{-1}, demonstrating the production of MgO nanoparticles [22]. Due to the interfacial bonding between Ag, MgO, and biochar, as shown in Figure 3, these all-organic molecules occurred in Ag/MgO@BC spectra, although with varying intensities. The result concluded that preparation of biochar with rice straw is entirely accountable for the AgNPs and MgONPs of reduction and stabilization on the surface of the modified biochar. The results clearly show the formation of Ag/MgO/biochar nanocomposites.

3.3. Zeta Potential. Zeta potential analysis is an important technique for analysing the surface morphological changes and stability of aqueous materials [21]. Charging variation on material surfaces can be affected by energy measurements. Often in micromolar strength, depending on the scale used for analysis, it is a very precise method for studying nanomaterials. It was observed from the Z potential results that the pure biochar nanocomposites had the highest concentration of bioactive ingredients at 28.4 mV, which is shown in Figure 4. After adding Ag/MgO to form the modified biochar composites, the zeta potential value changed to 29.2 mV, demonstrating that the MgO and Ag

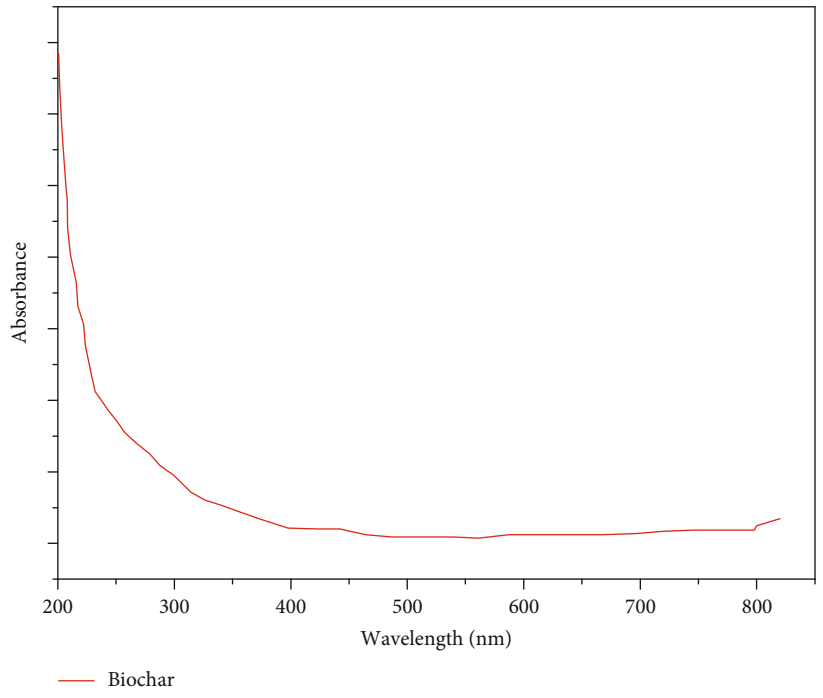

(a)

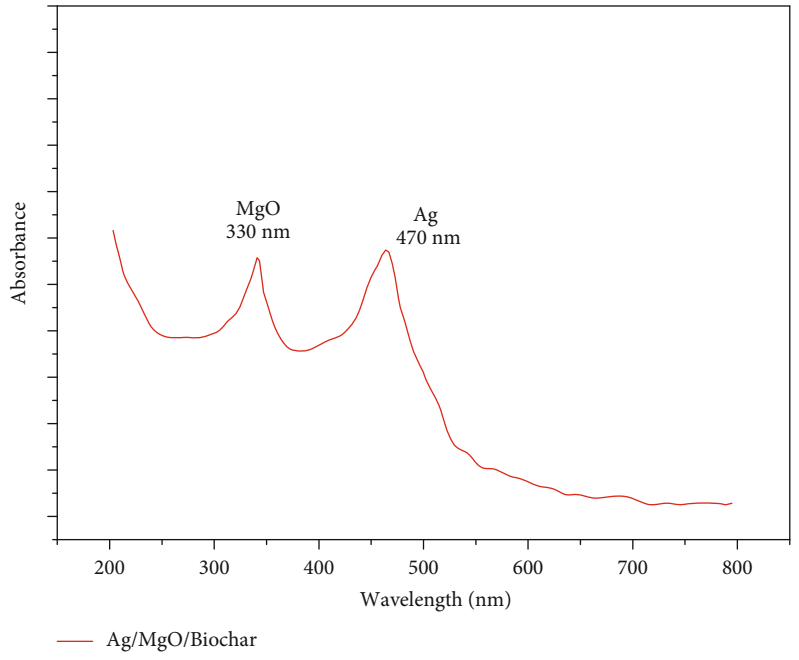

(b)

Figure 2: Continued.

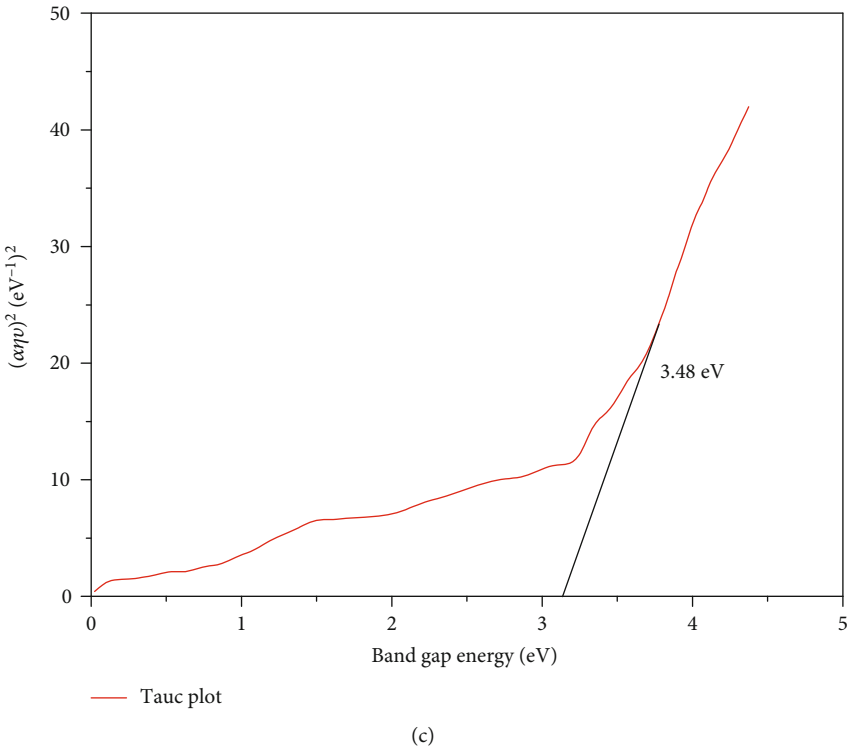

Figure 2: FTIR spectroscopy. (a) Biochar. (b) Ag/MgO/biochar. (c) Tauc Ag/MgO/biochar.

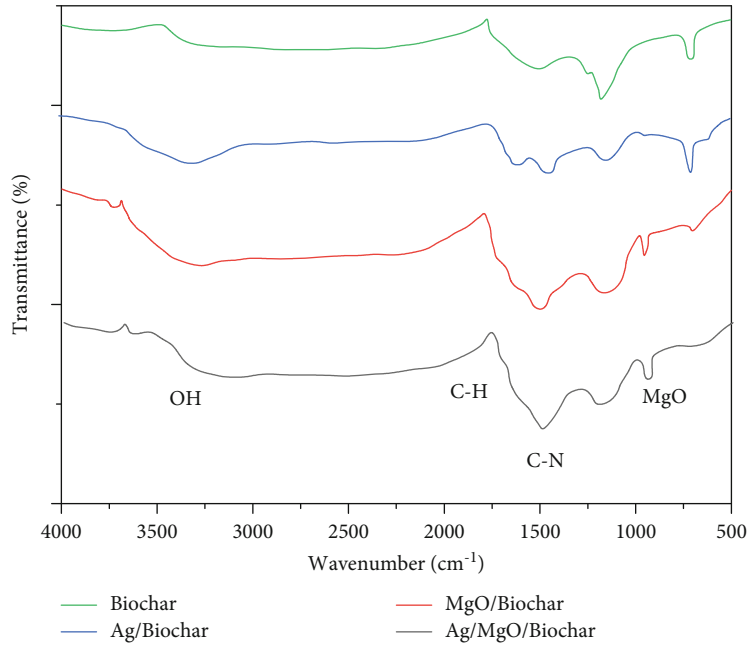

Figure 3: FTIR spectra.

nanoparticles on the biochar surface were activated successfully. The observed negative electrostatic potential can infer the stability of Ag/MgO@BC due to repulsive interactions between weakly charged ions [23].

3.4. SEM. The elemental presence of carbon especially develops with higher reaction temperature. EDX spectrum determined the different chemical constituents presented in biochar and their modified biochar nanocomposites. As shown in Figure 5, the EDX spectrum of pure biochar consists of elements C and O, which are anticipated the main components for typical biochar materials. Various elements considered major constituents of nanocomposites were also found in varying amounts, including C, Mg, Si, O, N, and

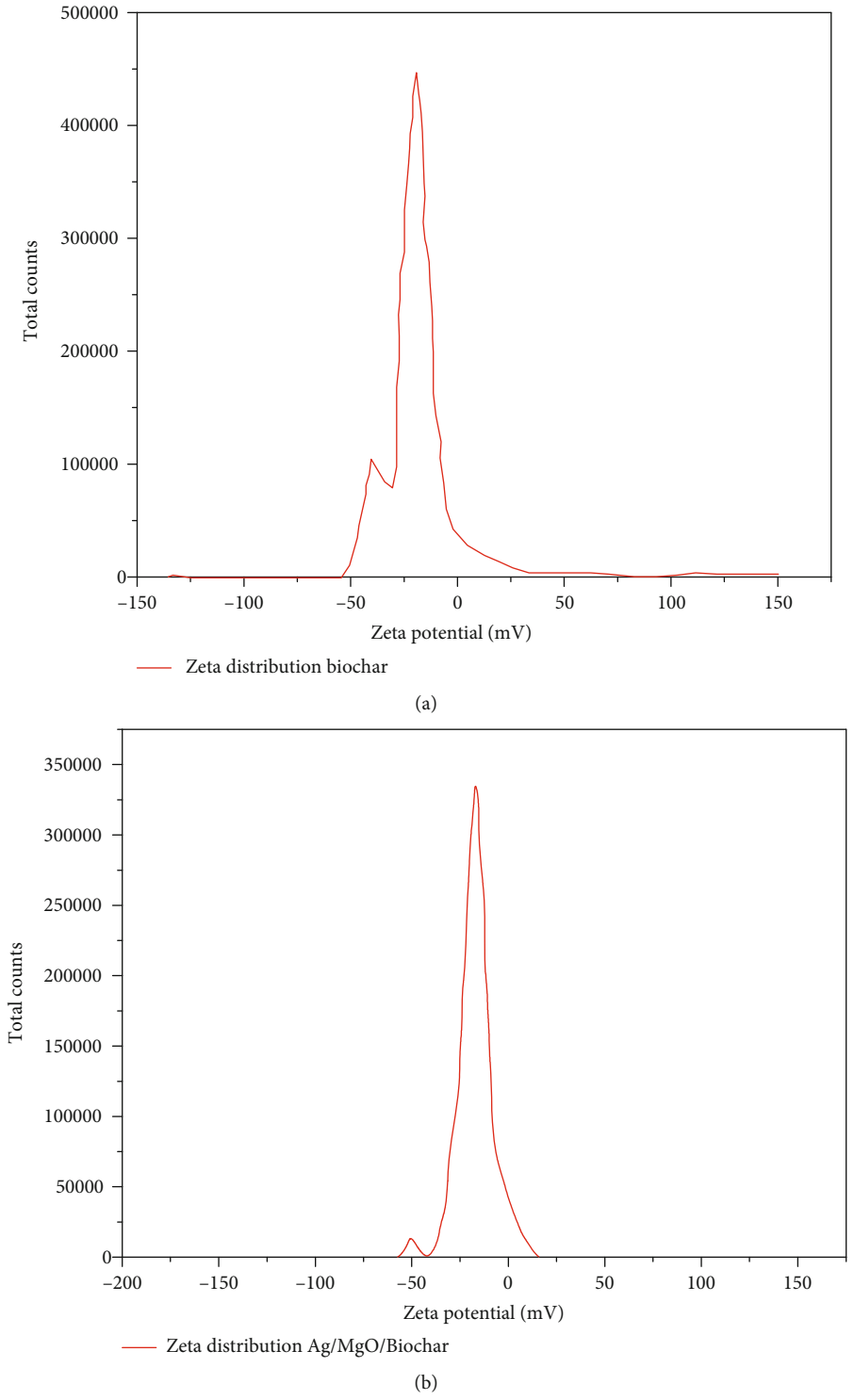

Figure 4: Zeta potential. (a) Biochar. (b) Ag/MgO/biochar.

k. Figures 5(a) and 5(b) show the EDS spectrum of all chemical elements available in Ag/MgO@BC nanocomposites [24]. Additionally, Mg-characteristic signals were observed in the same curve at energies of 0.9, 8.65, and 9.6 keV. These characteristics were determined according to Shaban et al. demonstrating the production of Ag/MgO@BC. Figure 5(b) shows the surface chemical composition of this biochar, which is 60.52% C, 2.15% Mg, 16.24.8% O, Ag 2.52%, and a small quantity of Si (0.7%). The lowest Ag % was 2.41%, and the essential MgO was 1.37%, corresponding to the proportion of magnesium oxide and silver ions (2%) according to EDX analysis of

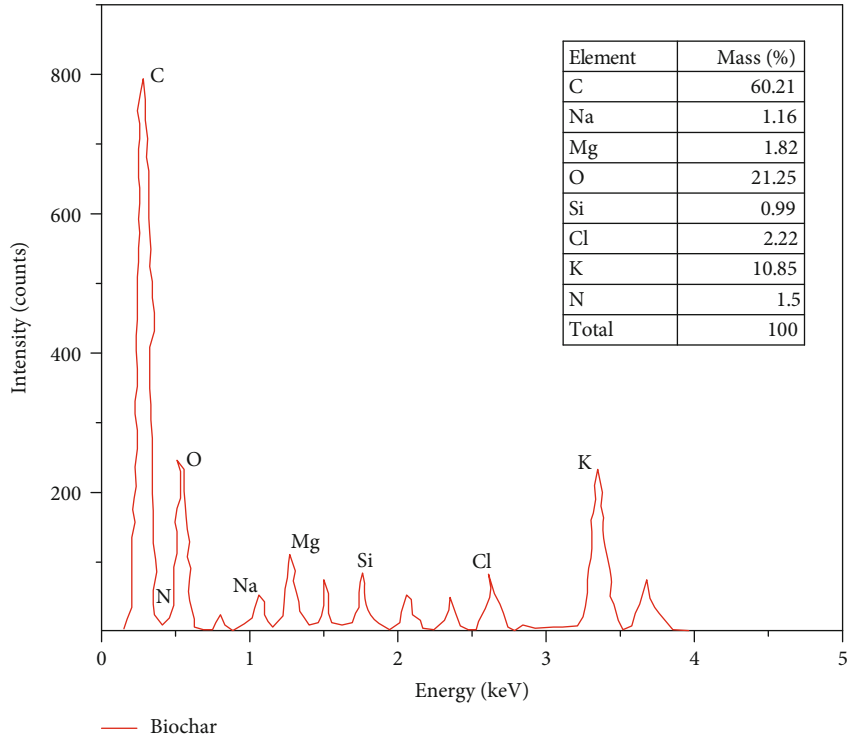

(a)

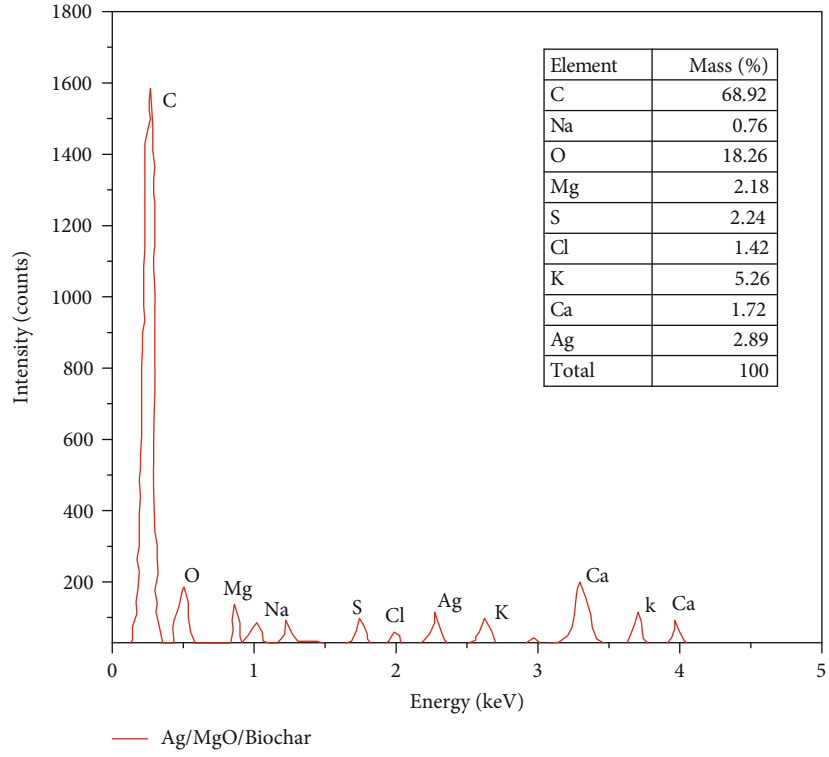

(b)

Figure 5: EDS spectrum of (a) biochar and (b) Ag/Mg/biochar.

the Ag/MgO @BCs surface. Biochar was initially applied to the surface to demonstrate the superior performance of rice straw extract in reducing zinc and silver ions.

The morphological changes and chemical % of elements of pure biochar and their Ag/MgO/biochar nanocomposites were characterized by using scanning electron microscope

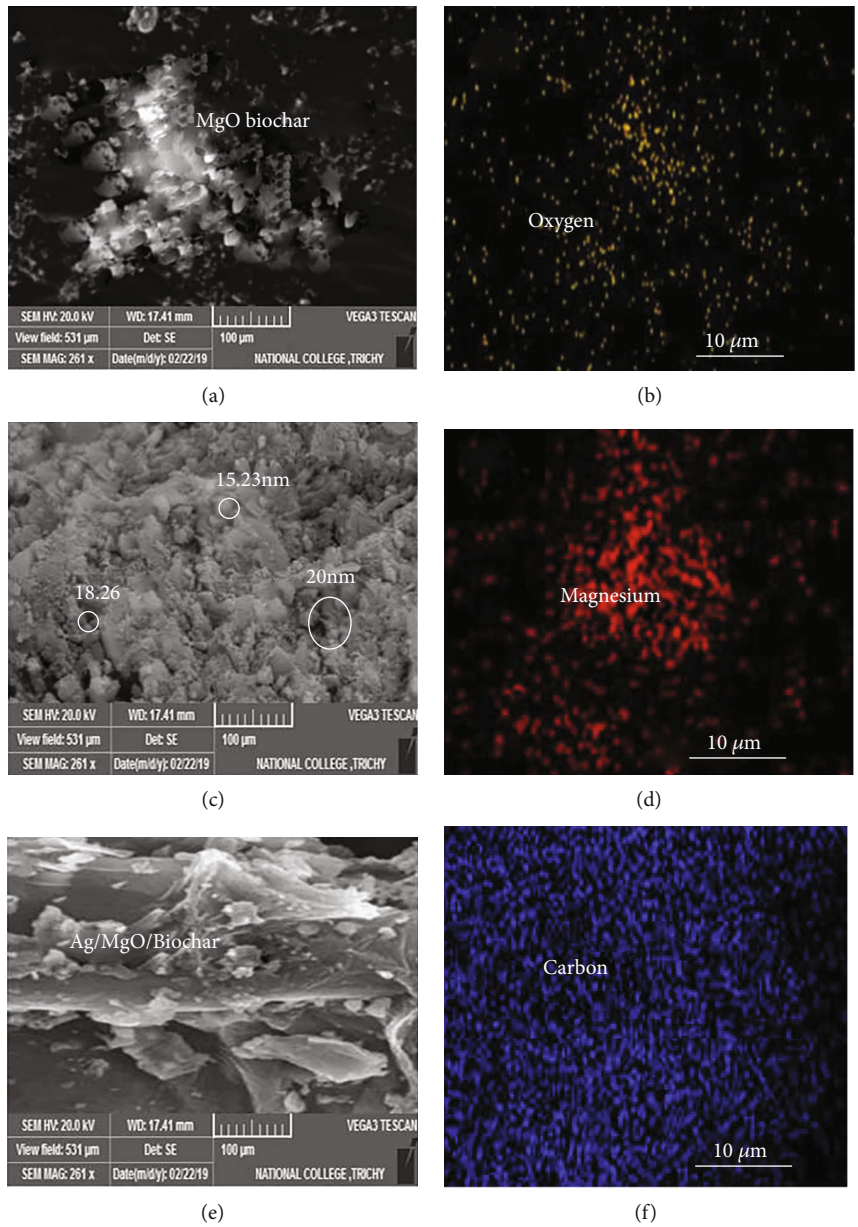

Figure 6: (a) MgO biochar. (b) Oxygen. (c) Ag/MgO/biochar. (d) Magnesium. (e) Ag/MgO/biochar. (f) Carbon.

(SEM) and energy dispersive spectrum (EDS), respectively. SEM is only useful for gathering information about surface morphology, but when combined with EDX, can be utilized to identify and quantify adherent nanoparticles. Figure 6(a) shows the MgO biochar elements in SEM. In this SEM, results revealed a pore structure during the thermal transesterification reaction, as porosity is widely believed to be caused by the emission of fine organic matter such as H_2O, CO_2, CH_4, and CO. This analysis also reveals the effect of AgNPs and MgONPs on biochar surface, porosity, size, and shape of the nanoparticles seen in Figure 6(b). The broad concentration of white nanoparticles on Ag/MgO@BC shown in Figures 6(c) and 6(d), which are not truly missing in biochar, suggests that MgONPs and AgNPs on the biochar surface were successfully ball milled (Figure 6(a)). Presence of Ag/MgO/biochar and carbon elements has been showed in Figures 6(e) and 6(f).

3.5. TEM Analysis. In this investigation, the size and morphology of photosynthesized AgNPs and MgONPs on activated carbon surfaces were examined using TEM analysis, frequently used to detect structural changes in prepared biochar nanoparticles. Figure 7(a) shows the TEM image of AgNPs and MgONPs on the biochar surface. TEM analysis clearly shows that the spherical shape of AgNPs and MgONPs was obtained up to 25 nm by using higher scales. The particle size obtained from TEM analysis agreed with SEM measurement, confirming effective ball milling synthesis techniques and determining the potential capability of different applications due to nanoparticle

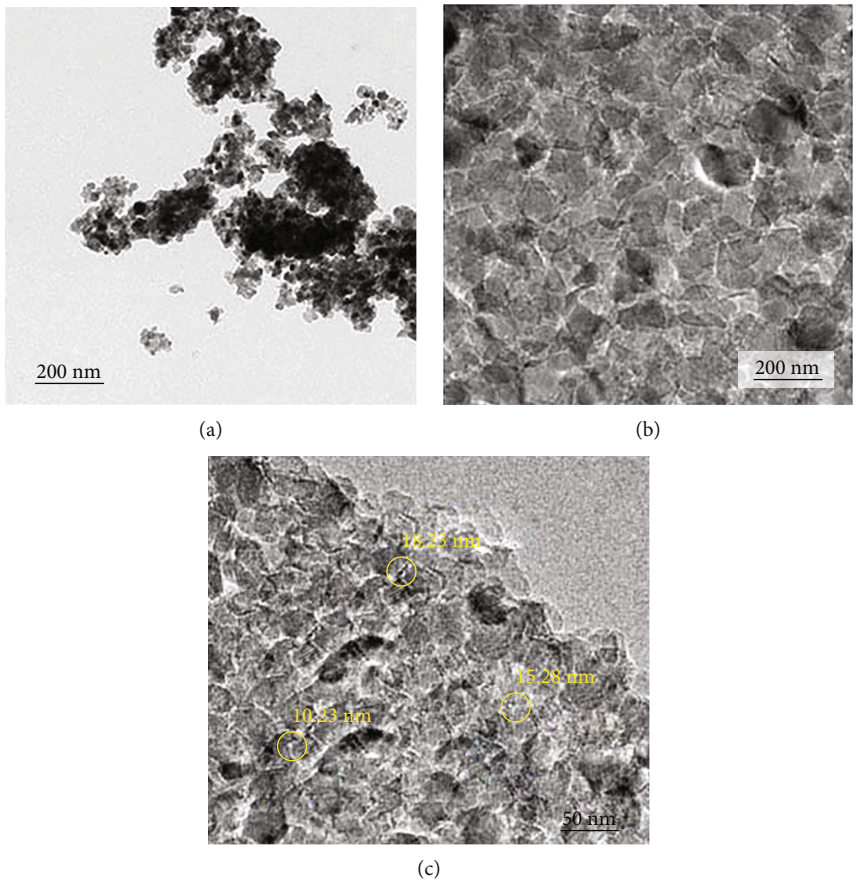

Figure 7: TEM images of Ag/MgO/biochar composites. (a) 200 nm. (b) MgONPs. (c) 100 nm modified biochar.

formation (Figure 7(b)). Figure 7(c) shows that the structure of MgO nanoparticles consists of nanostructures with random shapes and sizes of approximately 30 nm. Consistent with the results of Zheng et al. [21], they noted similar structures for Ag-composites with sizes ranging from 10 to 40 nm.

3.6. Thermal Gravity Analysis (TGA). Figure 8 shows pure biochar's thermal gravity analysis (TGA) and their reinforcement Ag/MgO/biochar nanocomposites. It exhibited a first continuous phase with a 10% weight loss up to 170°C, but the BC-prepared specimens showed an 8% weight loss, which could be attributed to moisture loss. Therefore, the temperature for biochar and Ag/MgO/biochar nanocomposites is 280°C and 352°, respectively. Significant weight loss between 320 and 460°C for Ag/MgO@BC sample and 330 and 450°C for BC nanocomposites can be attributed to the decomposition of major chemical elements. In conclusion, both samples experienced moderate weight loss up to 600°C, which may be due to the degrading lattice structure, although pure biochar weight loss was significant. However, Ag/MgO/BC experienced less overall weight loss than biochar, which may be attributed to the MgO NPs and AgNPs to withstand thermal degradation.

3.7. XRD Analysis. Figure 9 shows the XRD diffraction pattern of peak components of biochar and their nanocomposites. The XRD spectrum of silver nanoparticles shows the different peak intensities at 35^0, 42.65^0, 52.86^0, and 66.28^0 that are referenced from (111), (200), (220), and (311) planes subjected to face centred cubic (FCC) good agreed with the JCPDS file number 04-0783. The XRD diffraction patterns of Ag/MgO/biochar 32^0, 38.42^0, 45.32^0, and 52.18^0 have many characteristic patterns attributable to the (111), (200), (220), (311), and (222) plane crystalline structure that is identical to the peak of pure magnesium oxide nanoparticles according to JCPDS no. 87-0653. In addition, the (111) orientation is related to the formation orientation for ball-milled AgNPs at the interface of Ag/MgO/BC composites, in agreement with several other experimental works. The average crystalline size of nanoparticles was calculated by using the Debye Scherrer equation. The research showed that the MgO size of nanoparticles was reduced from 70 nm to 17 nm by ball milling with biochar. The MgO crystal structure produced from this investigation is comparable to the MgO improved biochar produced using the pyrolysis process. However, the results show that all AgNPs and MgONPs were successfully synthesized by ball milling on the biochar surface, yielding Ag/Mg/BC composites.

3.8. Antibacterial Activity. Bacteria Gram-positive and Gram-negative strain suppression abilities of Ag and MgO nanoparticles have been used in a spectrum of pharmacological activities. The antimicrobial potential of implanted

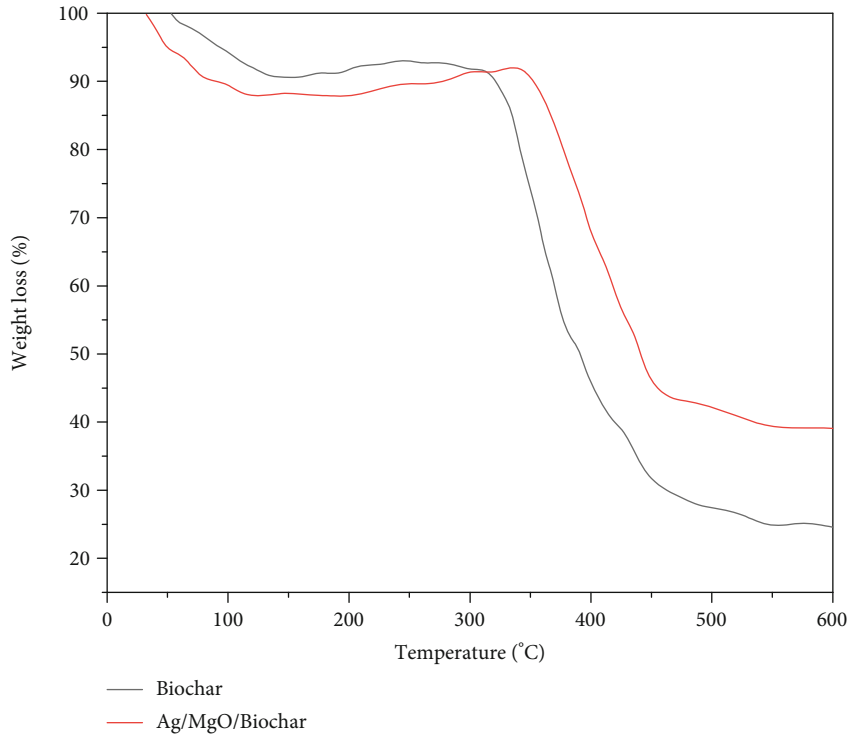

Figure 8: Thermal gravity analysis (TGA) of biochar and Ag/MgO/biochar nanocomposites.

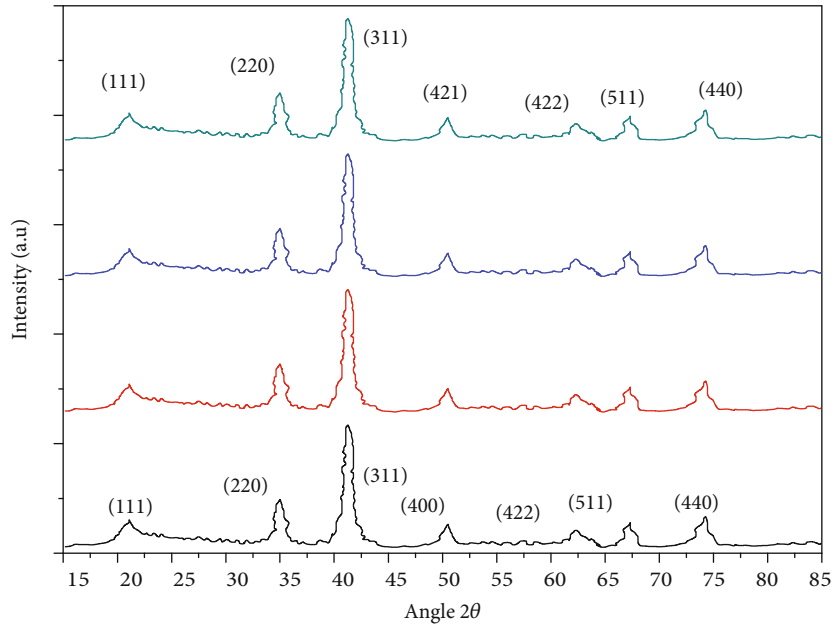

Figure 9: XRD diffraction pattern.

nanotechnology is thought to work in 2 phases: first, they inactivate thiol compounds in enzymes, and then, attach to the microbial chromosome, shorten it, and prevent DNA replication causing death [25]. The antibacterial activity of Ag/MgO@BC prepared nanocomposites throughout this research was then evaluated against a variety of Gram-positive and Gram-negative bacteria [26], including Escherichia coli pneumonia including S. aureus and E. coli species as shown in Figure 10. Research revealed that Ag/MgO@BC was a good antimicrobial treatment against pneumonia as it inhibited its growth at a large scale ($1x10^8$ CFU/mL) compared to other incorporated AgNPs and MgO/biochar nanocomposites. Figure 11 shows the zone of inhibition for both S. aureus and E. coli species of Ag/MgO@BC nanocomposites.

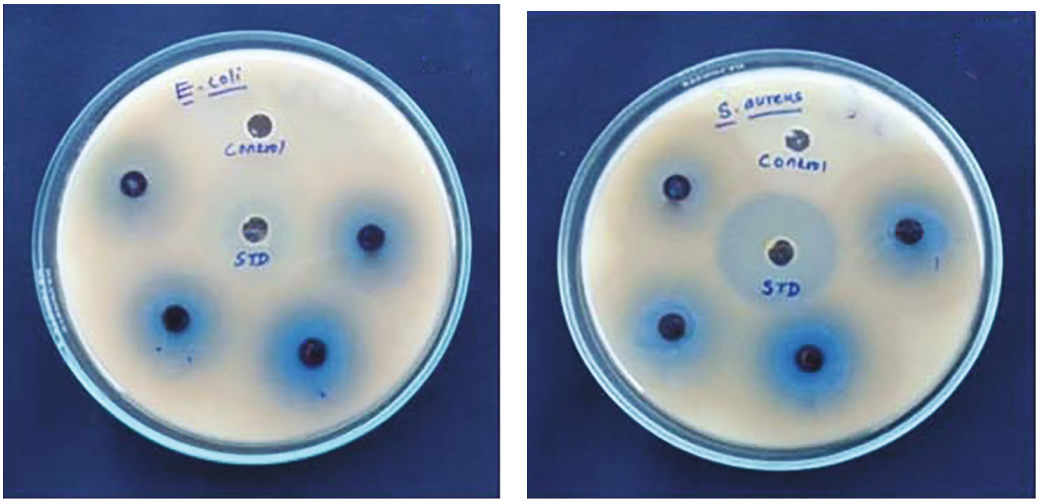

(a) (b)

Figure 10: Antibacterial activity Gram-positive and Gram-negative.

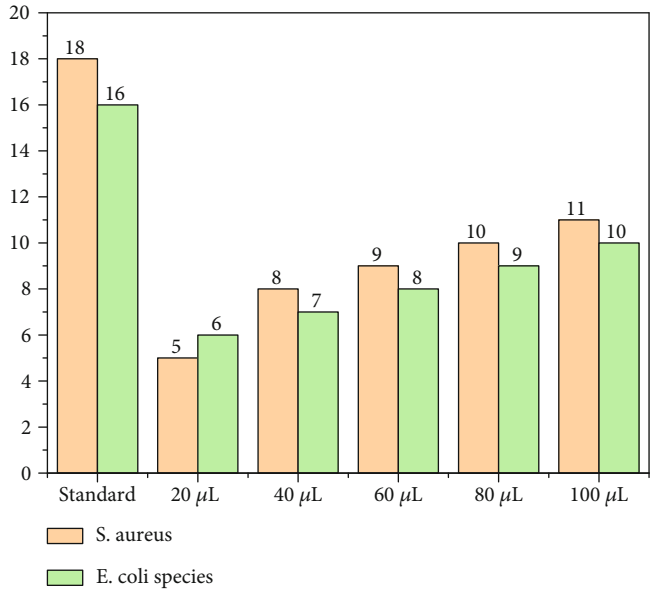

Figure 11: Zone of inhibition in mm antibacterial activity for Ag/MgO/biochar.

3.9. Adsorption Performance of Ag/MgO/Biochar Nanocomposites. Figures 12 and 13 show the adsorption performance of Ag/MgO/biochar nanocomposites. As small amounts of Mg/biochar were released from themselves, the aged biochar had limited MB and negative P adsorption. The P adsorption performance of Ag/MgO/Biochar was not affected by the ball-milling process, but the adsorption of MB was improved almost 8.4 times, which may be a result of higher surface area and pore size. The resulting Ag/MgO/biochar nanomaterials showed significantly enhanced adsorption of both P and MB. Strong Mg-P and Ag-P interfacial bonding and strong interaction between anionic P and electrically charged biochar surface during experimental parameters are responsible for enhanced P adsorption efficiency. The absorption properties of P removal have increased due to adding MgO to biochar composites. According to experimental results, Ag/MgO/biochar nanocomposites had charged positively membrane characteristics that aided in magnetic attractions and interfacial deposition of P ion species, which facilitated adsorption [27]. The MgO/biochar nanomaterials had MB absorption of 61.5 and 108.8% greater than pure biochar adsorption. The enhanced base neutralization ability of the biochar matrix [26], which is beneficial for removing ionic MB and attractive electrostatic stress at elevated pH levels, can be considered from the perspective of enhanced MB adsorption with Ag/MgO addition [25]. In the MgO/biochar nanocomposites specimens, MB sorption was initially enhanced and then diminished with MgO and concluded that there

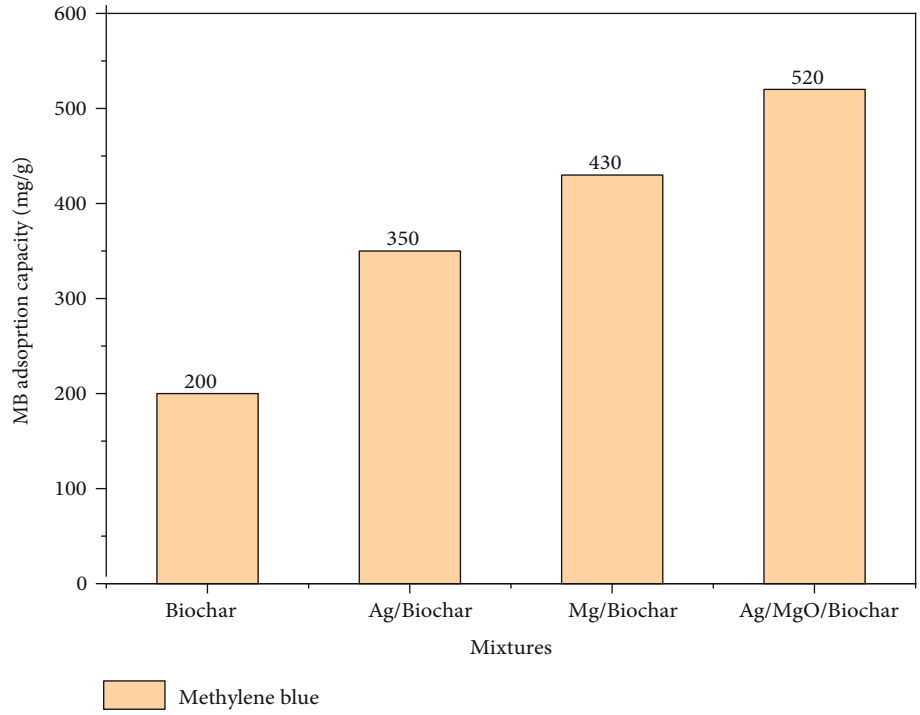

Figure 12: Removal of methylene blue.

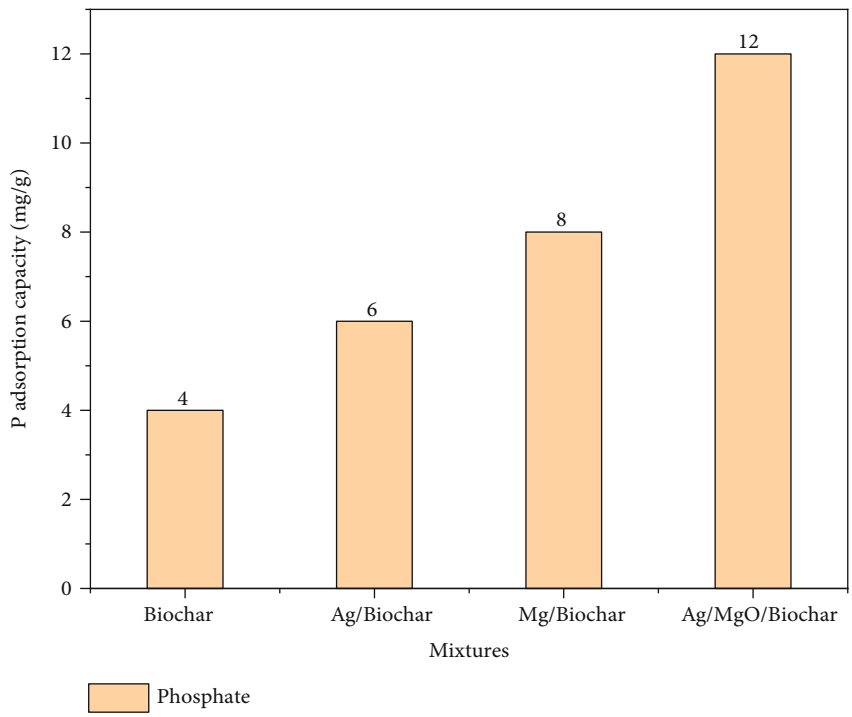

Figure 13: Removal of phosphate.

may be a perfect balance among MgO and biochar for removing contaminants [28]. Ag/MgO/biochar at 1 : 1 ratio of composites had the best P removal effectiveness in this work, combined with acceptable large efficiency for MB sorption [29].

3.10. Future Scope and Recommendations. Using biochar to remove contaminants from water is gaining significant popularity as an affordable alternative to expensive activated carbon [30]. Future research is needed to develop modified biochar to improve biochar quality, and its

performance varies depending on feedstock type and pyrolysis conditions [31]. It might be possible to modify biochar's characteristics to remove particular impurities to make it more efficient. Biochar has also been thoroughly explored as a cost-effective adsorbent for removing biological and metal pollutants from aqueous and gaseous atmospheric pollutants in environmental protection [32]. Although fresh biochar has a small adsorption capacity, different feed types and process conditions affect its physical and chemical properties (active adsorption sites, size distribution, and charge density) [33]. Consequently, it is necessary to develop techniques designed to regulate the concentration of biochar detection to improve its binding capacity to a range of environmental pollutants.

4. Conclusion

Synthesis of Ag/MgO@BC composites using rice straw biomass has been established for the first time in the present work using a scalable, cost-effective ball-milling method. This research demonstrates that the ball milling technique is a viable way to produce nanocomposite of metal oxides and biochar for wastewater treatment. The MgO was added into the biochar and uniformly dispersed, which improved the ability of the nanocomposites to bind MB and provide them with photocatalytic properties. According to experimental results, the ball-milling process provides more adaptability with efficiency on modified absorptions as well as structural modification achieved by synthesis techniques that strategically remove all biological and elemental contaminates. MB and PO_4^{3-} were successfully and synergistically removed from aqueous systems using Ag-added MgO-biochar nanocomposites.

FTIR analysis results found that MgO/biochar mixture also shows a unique MgO maximum intensity at 632 cm^{-1}, proving the synthesis of MgO nanoparticles. According to JCPDS no. 87-0653, the XRD diffraction patterns of Ag/MgO/Biochar 32^0, 38.42^0, 45.32^0, and 52.18^0 have numerous distinctive patterns that can be attributed to the crystal lattice of the (111), (200), (220), (311), and (222) planes, which is exactly equivalent to the peak of pure magnesium oxide nanoparticles. EDX analysis reveals that O, C, Mg, and Ag surface element content of 18.26%, 68.92%, 2.18%, and 2.89%, respectively. The elemental analysis of Ag/MgO@BC observed that the percentage of Ag is 2.89% and Mg is 2.18%, which is close to the percentage of MgO and silver ions. Most ball-milled nanoparticles have 10 to 40 nm on the spherical surface of Ag/MgO@BC nanocomposites. Zeta potential of 28.4 mV has been used to indicate sustainability, and Ag/ZnO@BC showed high efficiency. When compared to other integrated AgNPs and MgO/Biochar nanocomposites, the analysis revealed that Ag/MgO@BC prevented the development of pneumonia at a high scale (1×10^8 CFU/mL).

Modified biochar Ag/ZnO@BC exhibited significant antibacterial activity towards S. aureus and E. coli species bacteria, with high productivity of 40% at the highest concentration (100 g/mL). Evaluation of some alternative green-synthesized AgNPs, MgONPs, and their nanostructured materials revealed that Ag/MgO@BC is a potent antibacterial agent against gram-positive and gram-negative because of a large dosage (2×10^8 CFU/mL). Consequently, the zone of inhibition was 11 mm against S. aureus and 10 mm for E. coli antibacterial activity. Combining Ag/MgO@BC is a unique nanocomposite that can be effectively used for a wide range of environmental and therapeutic applications.

Data Availability

The data used to support the findings of this study are included within the article. Should further data or information be required, these are available from the corresponding author upon request.

Conflicts of Interest

The authors declare that there are no conflicts of interest regarding the publication of this paper.

References

[1] Y. Xiao, H. Lyu, J. Tang, K. Wang, and H. Sun, "Effects of ball milling on the photochemistry of biochar: enrofloxacin degradation and possible mechanisms," *Chemical Engineering Journal*, vol. 384, article 123311, 2020.

[2] R. Li, J. J. Wang, L. A. Gaston et al., "An overview of carbothermal synthesis of metal-biochar composites for the removal of oxyanion contaminants from aqueous solution," *Carbon*, vol. 129, pp. 674–687, 2018.

[3] M. Hosny, "Biogenic synthesis, characterization, antimicrobial, antioxidant, and catalytic applications of synthesized platinum nanoparticles (PtNPs) from Polygonum salicifolium leaves," *Journal of Environmental Chemical Engineering*, vol. 10, article 106806, 2022.

[4] E. M. Abd El-Monaem, A. S. Eltaweil, H. M. Elshishini et al., "Sustainable adsorptive removal of antibiotic residues by chitosan composites: an insight into current developments and future recommendations," *Arabian Journal of Chemistry*, vol. 15, no. 5, article 103743, 2022.

[5] J. Kruse, M. Abraham, W. Amelung et al., "Innovative methods in soil phosphorus research: a review," *Journal of Plant Nutrition and Soil Science*, vol. 178, no. 1, pp. 43–88, 2015.

[6] C. Tarayre, L. De Clercq, R. Charlier et al., "New perspectives for the design of sustainable bioprocesses for phosphorus recovery from waste," *Bioresource Technology*, vol. 206, pp. 264–274, 2016.

[7] R. Li, J. J. Wang, B. Zhou et al., "Recovery of phosphate from aqueous solution by magnesium oxide decorated magnetic biochar and its potential as phosphate-based fertilizer substitute," *Bioresource Technology*, vol. 215, pp. 209–214, 2016.

[8] R. Li, J. J. Wang, B. Zhou et al., "Enhancing phosphate adsorption by Mg/Al layered double hydroxide functionalized biochar with different Mg/Al ratios," *Science of the Total Environment*, vol. 559, pp. 121–129, 2016.

[9] T. T. Li, Z. H. Tong, B. Gao, Y. C. C. Li, A. Smyth, and H. K. Bayabil, "Polyethyleneimine-modified biochar for enhanced phosphate adsorption," *Environmental Science and Pollution Research*, vol. 27, no. 7, pp. 7420–7429, 2020.

[10] F. Yu, F. Y. Tian, H. W. Zou et al., "ZnO/biochar nanocomposites via solvent free ball milling for enhanced adsorption and photocatalytic degradation of methylene blue," *Journal of Hazardous Materials*, vol. 415, article 125511, 2021.

[11] X. Zhang, K. Ren, Y. T. Wang, B. X. Shen, F. Shen, and Y. Shang, "Solvent-free synthesis of MnOx-FeOx/biochar for Hg0ando-xylene removal from flue gas," *Energy & Fuels*, vol. 35, no. 19, pp. 15969–15977, 2021.

[12] M. Kumar, X. Xiong, Z. Wan et al., "Ball milling as a mechanochemical technology for fabrication of novel biochar nanomaterials," *Bioresource Technology*, vol. 312, article 123613, 2020.

[13] S. O. Amusat, T. G. Kebede, S. Dube, and M. M. Nindi, "Ball-milling synthesis of biochar and biochar-based nanocomposites and prospects for removal of emerging contaminants: a review," *ournal of Water Process Engineering*, vol. 41, article 101993, 2021.

[14] B. Wang, B. Gao, and Y. S. Wan, "Entrapment of ball-milled biochar in Ca-alginate beads for the removal of aqueous Cd(II)," *Journal of Industrial and Engineering Chemistry*, vol. 61, pp. 161–168, 2018.

[15] Y. F. Li, A. R. Zimmerman, F. He et al., "Solvent-free synthesis of magnetic biochar and activated carbon through ball- mill extrusion with Fe_3O_4 nanoparticles for enhancing adsorption of methylene blue," *Science of The Total Environment*, vol. 722, article 137972, 2020.

[16] X. Xu, Y. Zheng, B. Gao, and X. Cao, "N-doped biochar synthesized by a facile ball-milling method for enhanced sorption of CO_2 and reactive red," *Chemical Engineering Journal*, vol. 368, pp. 564–572, 2019.

[17] D. Liu, G. Li, J. Liu, and Y. Yi, "Organic-inorganic hybrid mesoporous titanium silica material as bi-functional heterogeneous catalyst for the CO_2 cycloaddition," *Fuel*, vol. 244, pp. 196–206, 2019.

[18] P. S. Kumar, R. N. Kamath, P. Boyapati, P. J. Josephson, L. Natrayan, and F. D. Shadrach, "IoT battery management system in electric vehicle based on LR parameter estimation and ORMeshNet gateway topology," *Sustainable Energy Technologies and Assessments*, vol. 53, article 102696, 2022.

[19] S. Saedi, M. Shokri, J. T. Kim, and G. H. Shin, "Semi-transparent regenerated cellulose/ZnONP nanocomposite film as a potential antimicrobial food packaging material," *Journal of Food Engineering*, vol. 307, article 110665, 2021.

[20] E. Gurgur, S. Oluyamo, A. Adetuyi, O. Omotunde, and A. Okoronkwo, "Green synthesis of zinc oxide nanoparticles and zinc oxide–silver, zinc oxide–copper nanocomposites using Bridelia ferruginea as bio template," *SN Applied Sciences*, vol. 2, pp. 1–12, 2020.

[21] Y. Zheng, Y. Yang, Y. Zhang et al., "Facile one-step synthesis of graphitic carbon nitride-modified biochar for the removal of reactive red 120 through adsorption and photocatalytic degradation," *Biochar*, vol. 1, no. 1, pp. 89–96, 2019.

[22] M. Ponnusamy, L. Natrayan, P. P. Patil, G. Velmurugan, and Y. T. Keno, "Statistical analysis on interlaminar shear strength of nanosilica addition with woven dharbai/epoxy hybrid nanocomposites under cryogenic environment by Taguchi technique," *Adsorption Science & Technology*, vol. 2022, article 6571515, 9 pages, 2022.

[23] T. Bhuyan, K. Mishra, M. Khanuja, R. Prasad, and A. Varma, "Biosynthesis of zinc oxide nanoparticles from *Azadirachta indica* for antibacterial and photocatalytic applications," *Materials Science in Semiconductor Processing*, vol. 32, pp. 55–61, 2015.

[24] Y. Khimsuriya, D. K. Patel, Z. Said et al., "Artificially roughened solar air heating technology - a comprehensive review," *Applied Thermal Engineering*, vol. 214, article 118817, 2022.

[25] A. Z. Hassan, A. W. M. Mahmoud, G. M. Turky, and G. Safwat, "Rice husk derived biochar as smart material loading nano nutrients and microorganisms," *Bulgarian Journal of Agricultural Science*, vol. 26, pp. 309–322, 2020.

[26] M. M. Matheswaran, T. V. Arjunan, S. Muthusamy et al., "A case study on thermo-hydraulic performance of jet plate solar air heater using response surface methodology," *Thermal Engineering*, vol. 34, article 101983, 2022.

[27] A. S. Eltaweil, A. M. Abdelfatah, M. Hosny, and M. Fawzy, "Novel biogenic synthesis of a Ag@biochar nanocomposite as an antimicrobial agent and photocatalyst for methylene blue degradation," *ACS Omega*, vol. 7, no. 9, pp. 8046–8059, 2022.

[28] Z. Ma, J. Liu, Y. Liu, X. Zheng, and K. Tang, "Green synthesis of silver nanoparticles using soluble soybean polysaccharide and their application in antibacterial coatings," *International Journal of Biological Macromolecules*, vol. 166, pp. 567–577, 2021.

[29] L. Natrayan, D. Veeman, P. P. Patil, V. S. Nadh, P. Balamurugan, and M. D. Chewaka, "Surface state treatment of carbon dots using sulphur dioxide isotherm," *Adsorption Science & Technology*, vol. 2022, article 7387409, 9 pages, 2022.

[30] Y. Yao, B. Gao, J. Chen, and L. Yang, "Engineered biochar reclaiming phosphate from aqueous solutions: mechanisms and potential application as a slow-release fertilizer," *Environmental Science & Technology*, vol. 47, no. 15, pp. 8700–8708, 2013.

[31] M. Hosny, M. Fawzy, and A. S. Eltaweil, "Green synthesis of bimetallic Ag/ZnO@Biohar nanocomposite for photocatalytic degradation of tetracycline, antibacterial and antioxidant activities," *Scientific Reports*, vol. 12, no. 1, pp. 1–17, 2022.

[32] M. Ponnusamy, L. Natrayan, P. P. Patil, G. Velmurugan, and S. Thanappan, "Multiresponse optimization of mechanical behaviour of Calotropis gigantea/nano-silicon-based hybrid nanocomposites under cryogenic environment," *Adsorption Science & Technology*, vol. 2022, article 4138179, 14 pages, 2022.

[33] S. Lokina, A. Stephen, V. Kaviyarasan, C. Arulvasu, and V. Narayanan, "Cytotoxicity and antimicrobial activities of green synthesized silver nanoparticles," *European Journal of Medicinal Chemistry*, vol. 76, pp. 256–263, 2014.